From Calcium to Cadmium: Testing the Pairing Functional through Charge Radii Measurements of $^{100-130}$Cd

M. Hammen,[1] W. Nörtershäuser,[1,2,*] D. L. Balabanski,[3,†] M. L. Bissell,[6,8] K. Blaum,[5] I. Budinčević,[6] B. Cheal,[7] K. T. Flanagan,[8] N. Frömmgen,[1] G. Georgiev,[9] Ch. Geppert,[1,2] M. Kowalska,[4] K. Kreim,[5] A. Krieger,[1,2] W. Nazarewicz,[10] R. Neugart,[1,5] G. Neyens,[4,6] J. Papuga,[6] P.-G. Reinhard,[11] M. M. Rajabali,[6,‡] S. Schmidt,[1,2] and D. T. Yordanov[4,5,12]

[1]Institut für Kernchemie, Johannes Gutenberg-Universität Mainz, Fritz-Straßmann Weg 2, 55128 Mainz, Germany
[2]Institut für Kernphysik, Technische Universität Darmstadt, Schlossgartenstraße 9, 64289 Darmstadt, Germany
[3]INRNE, Bulgarian Academy of Science, BG-1784 Sofia, Bulgaria
[4]CERN European Organization for Nuclear Research, Physics Department, CH-1211 Geneva 23, Switzerland
[5]Max-Planck-Institut für Kernphysik, Saupfercheckweg 1, 69117 Heidelberg, Germany
[6]Instituut voor Kern- en Stralingsfysica, KU Leuven, Celestijnenlaan 200D, B-3001 Leuven, Belgium
[7]Oliver Lodge Laboratory, University of Liverpool, Liverpool, L69 7ZE, United Kingdom
[8]Photon Science Institute, School of Physics and Astronomy, University of Manchester, Manchester, M13 9PL, United Kingdom
[9]CSNSM-IN2P3-CNRS, Université de Paris Sud, F-91405 Orsay, France
[10]Department of Physics and Astronomy and FRIB Laboratory, Michigan State University, East Lansing, Michigan 48824, USA
[11]Institut für Theoretische Physik II, Universität Erlangen-Nürnberg, 91058 Erlangen, Germany
[12]Institut de Physique Nucléaire, CNRS-IN2P3, Université Paris-Sud, Université Paris-Saclay, F-91406 Orsay, France

Differences in mean-square nuclear charge radii of $^{100-130}$Cd are extracted from high-resolution collinear laser spectroscopy of the $5s\,^2S_{1/2} \rightarrow 5p\,^2P_{3/2}$ transition of the ion and from the $5s5p\,^3P_2 \rightarrow 5s6s\,^3S_1$ transition in atomic Cd. The radii show a smooth parabolic behavior on top of a linear trend and a regular odd-even staggering across the almost complete $sdgh$ shell. They serve as a first test for a recently established new Fayans functional and show a remarkably good agreement in the trend as well as in the total nuclear charge radius.

The radius is one of the most fundamental properties of a nucleus. The general trend that radii increase roughly with $A^{1/3}$ was already extracted from early studies using nuclear reactions and elastic electron scattering and gave rise to the famous liquid drop model assuming a constant saturation density inside the nucleus [1,2]. Electron scattering experiments reveal not only the overall extension of a nucleus but also the whole charge density distribution [3] which then can be characterized by several form parameters such as the diffraction radius, surface thickness, and root-mean-square (rms) radius [4]. A variety of experimental approaches have been used to measure the rms radius, and there now exists a rich collection of data across the nuclear chart, see, e.g., [5,6]. In the following, we consider only rms nuclear charge radii and call them simply radii. Precision measurements of charge radii by optical spectroscopy reveal many facets of nuclear structure and dynamics along chains of isotopes

[7,8]. The most prominent one is probably the kink at a shell closure, but even more pronounced are sometimes sudden shape changes, occurring with the addition of a single neutron when collective effects drive the nucleus from a spherical into a deformed shape or back. The odd-even staggering between nuclei with consecutive odd and even neutron numbers is a more subtle behavior. It can be explained, in principle, by the blocking effect of the odd nucleon. But a quantitative, theoretical understanding of odd-even effects is still an open problem [9–11]. The difference between the radii of neutron and proton distributions (directly related to charge radius) can be understood in terms of a neutron skin, which has been shown to be correlated with a number of other observables in finite nuclei as well as in nuclear and neutron matter [12–14]. Hence, precision measurements of charge radii as presented in this study can provide complementary information, e.g., about basic nuclear matter properties [15] or the dipole polarizability in nuclei [16].

One of the most ambitious goals of nuclear structure theory is a global description of nuclear charge radii, i.e., its trend over all nuclear sizes as well as local variations along isotopic chains. In light nuclei, radii are strongly affected by their cluster structure [17] and correlation effects [18].

Here, A-body methods based on realistic internucleon interactions have made enormous progress [19], and the data on charge radii turned out to be essential for constraining nuclear saturation [15,20]. The tool of choice for a microscopic description of nuclei throughout the whole mass table is nuclear density functional theory (DFT), which has been particularly successful in the medium and heavy mass region [21]. Charge radii along the isotopic chain of calcium, a long standing problem in nuclear physics, have been addressed by these techniques, and radii of ^{40}Ca and ^{48}Ca could be described quite well based on the realistic functionals. However, none of the theories could accommodate for the detailed trends as the fast increase of the nuclear charge radius from ^{48}Ca to ^{52}Ca [22] or the intricate behavior of charge radii between ^{40}Ca and ^{48}Ca. In order to improve the description of isotopic trends, particularly the odd-even staggering, in DFT, the Fayans functional was developed which includes also a gradient term in the pairing functional [23,24]. The functional was taken up and further tuned to improve the agreement with the experiment along the calcium chain up to ^{52}Ca [25] and reproduces also charge radii of iron isotopes around $N = 28$ [26]. In an alternative branch of nuclear DFT, a relativistic density functional approach has been employed with a Bayesian neural network (FSUGarnet + BNN) in order to provide an improved description of charge radii [27]. This also leads to a reasonable trend along the Ca isotopes but cannot accommodate the odd-even staggering. In view of these ongoing developments, new precision data on radii along long isotopic chains are essential.

Here, we present new results of charge radii of Cd isotopes, with $Z = 48$ one proton pair below the $Z = 50$ proton shell closure. We have studied transitions in the neutral atom as well as in the singly charged ion and extracted a set of charge radii along almost the complete $sdgh$ shell from ^{100}Cd ($N = 52$) up to the shell closure at ^{130}Cd ($N = 82$). We compare our results with predictions from relativistic and nonrelativistic DFT. We find a remarkably good agreement for the absolute size as well as the trend along the isotopic chain for the Fayans functional parametrization optimized to the change in the mean square charge radii of calcium isotopes. In comparison, the relativistic FSUGarnet + BNN approach follows roughly the trend but cannot reproduce details.

The experiments were conducted with the collinear laser spectroscopy apparatus COLLAPS at the radioactive ion beam facility ISOLDE/CERN [28]. Neutron-rich isotopes of Cd were produced by a 1.4-GeV proton beam impinging on a tungsten rod which serves as a neutron converter located next to a UC$_x$ target. To further suppress beam contamination from cesium isobars, a quartz transfer line [29] was implemented between the target and the hot cavity where resonant laser ionization was applied to selectively generate Cd$^+$ ions. Neutron-deficient isotopes were produced in a separate run by proton-induced spallation in a

molten Sn target combined with a plasma ion source. The ions were accelerated to 30 keV and mass separated, prior to study using the COLLAPS beam line [30].

Singly charged ions (Cd II) were excited in the $5s\,^2S_{1/2} \to 5p\,^2P_{3/2}$ transition using laser light at 214.5 nm copropagating with the ion beam, while for neutral atoms (Cd I) the $5s5p\,^3P_2 \to 5s6s\,^3S_1$ transition at 508.7 nm was used. Resonance lines were recorded using Doppler tuning of the ion velocity by a reacceleration potential applied to either the charge exchange cell or the fluorescence detection region for atomic and ionic spectroscopy, respectively. The detection region was described previously [31] and has been equipped with four photomultiplier tubes and UV-compatible optics to allow for efficient detection of the 215-nm fluorescence photons of the ions. The spectroscopy on neutral atoms was performed with continuous beams delivered from the ISOLDE general-purpose separator and was restricted to $^{106-124,126}$Cd. Studies on Cd II were performed with bunched and cooled beams from ISCOOL [32] at the high-resolution separator using accumulation times of typically 200 ms and ion bunches of approximately 5-μs temporal width. The light detection gate was triggered with the arrival time of the ion bunch at the detection region and gated for the measured time width of the ion bunch to suppress background from scattered laser light by about 4 orders of magnitude. This allowed us to extend the range of measurements up to ^{130}Cd and altogether cover the complete $sdgh$ shell with the exception of ^{99}Cd. More details on the collinear spectroscopy on Cd I [33] and Cd II [34,35] are provided in previous publications in which the nuclear moments [33,34] and the isomer shifts [35] are addressed.

The deep-UV continuous-wave laser light required for spectroscopy on the 214.5-nm line in Cd II was produced by frequency quadrupling of a titanium-sapphire laser using two frequency-doubling stages. In total, about 5 mW UV light was produced from 1.2 W output power at 859 nm of a titanium-sapphire laser, pumped with 8 W at 532 nm delivered from a solid state laser. The titanium-sapphire frequency was stabilized to a stable helium-neon laser via a transfer cavity, and the wavelength was recorded by a high-precision wave meter.

The analysis of the spectra obtained in the Cd I transition has been discussed in detail in [33]. The Cd II spectra were treated similarly: they were fitted with a hyperfine spectrum using Voigt profiles for each component. In order to reduce the number of free parameters, the Lorentzian linewidth was kept fixed to the natural linewidth of the transition (45 MHz), while the Gaussian component width was extracted from the corresponding spectrum of the reference isotope ^{114}Cd. Moreover, the ratio of the A factors of the $5s\,^2S_{1/2}$ and the $5p\,^2P_{3/2}$ state was fixed to the average value observed in the stable odd isotopes. Since the A factor in the upper state is about 30 times smaller than the one in the ground state, the effect of a possible hyperfine-structure

anomaly is expected to be within the statistical uncertainty. This procedure avoids uncertainties caused by a strong correlation between a free upper-state A factor and the corresponding B factor, especially for the isotope ^{107}Cd. For ^{129}Cd, relative line intensities were fixed to those observed for the corresponding ^{125}Cd spectra to compensate for the low statistics and an overlap of the spectral structures arising from the ground and the isomeric state. These spectra of both isotopes were recorded with similar laser power to provide for a comparable effect of optical pumping on the line intensities. Spin assignments, extracted nuclear moments, and isomer shifts were published previously [34,35]. The isotope shift for each spectrum is calculated relative to the position of the reference isotope ^{114}Cd. In order to take into account possible drifts of the laser frequency, the high voltage, or the gas pressure in ISCOOL, reference spectra recorded immediately before and after data-taking on the short-lived isotope were averaged. The results were used to interpolate the reference position during the measurement of the short-lived isotope. All individual measurements from two running periods were averaged, weighted with their statistical uncertainty. The results are listed in Table I, including also the isotope shifts measured in the Cd I line. The high voltage of ISCOOL was regularly recorded during the beam time and compared with the resonance position of the reference isotope to verify stability of voltage and laser frequency. Because of experimental difficulties during the last hours of beamtime, additional results for the isotopes $^{117–120,122}$Cd on the Cd II transition are not available. Hence, the charge radii of these isotopes were extracted from the Cd I transition.

The relation between the isotope shift $\delta\nu^{A,A'}$ and the nuclear size is

$$\delta\nu^{A,A'} := \nu^{A'} - \nu^{A} = F\lambda^{A,A'} + K\mu, \qquad (1)$$

where $\mu = (m_{A'} - m_A)/(m_A \times m_{A'})$ is the mass factor and K and F are the mass-shift and the electronic field-shift constants of the transition, respectively. The nuclear size parameter $\lambda^{A,A'} = \delta\langle r^2\rangle^{A,A'} + C_2/C_1\delta\langle r^4\rangle^{A,A'} + C_3/C_1\delta\langle r^6\rangle^{A,A'}$ takes into account $\delta\langle r^2\rangle$ and higher moments of the nuclear charge distribution. For Cd, the Seltzer coefficients are $C_2/C_1 = -5.96 \times 10^{-4}$ fm^{-2} and $C_3/C_1 = 1.88 \times 10^{-6}$ fm^{-4} [5]. While the mass factor μ can be based on precise isotope masses [36], F and K were obtained from a King plot procedure as described, e.g., in [37]: Equation (1) is transformed into the linear relation

$$\delta\nu_{\text{mod}}^{A,A'} = F\lambda_{\text{mod}}^{A,A'} + K, \quad \text{with} \quad [\lambda, \delta\nu]_{\text{mod}} = \mu^{-1}[\lambda, \delta\nu]. \quad (2)$$

The "modified" size parameters $\lambda_{\text{mod}}^{A,A'}$ are determined for the stable isotopes from a combined analysis of muonic atom and electron scattering data [37]. Changes in the mean square

TABLE I. Spins I, isotope shifts $\delta\nu^{114,A}$ in the $5s\,^2S_{1/2} \to 5p\,^2P_{3/2}$ (Cd II), and the $5s5p\,^3P_2 \to 5s6s\,^3S_1$ (Cd I) transitions and extracted differences in mean-square charge radii $\delta\langle r^2\rangle^{114,A}$ of the measured cadmium isotopes with respect to ^{114}Cd. Radii were extracted from the Cd II data with the exception of $^{117–120,122}$Cd for which information from this transition is missing. Uncorrelated uncertainties are in parentheses, correlated ones in brackets. A -2.7% contribution of higher radial moments has been assumed in the extraction of $\delta\langle r^2\rangle^{114,A}$ from $\lambda^{114,A}$.

A	I	$\delta\nu_{\text{Cd II}}^{114,A}$ (MHz)	$\delta\nu_{\text{Cd I}}^{114,A}$ (MHz)	$\delta\langle r^2\rangle^{114,A}$ (fm^2)
100	0	6371.6(31)[114]		−1.421(5)[043]
101	5/2	5859.9(22)[105]		−1.307(4)[040]
102	0	5037.2(22)[096]		−1.144(3)[025]
103	5/2	4621.6(24)[087]		−1.046(3)[024]
104	0	3922.7(24)[079]		−0.904(2)[016]
105	5/2	3608.7(22)[070]		−0.823(2)[016]
106	0	2991.1(22)[062]	−800.9(18)[31]	−0.695(2)[012]
107	5/2	2730.9(23)[054]	−724.0(13)[25]	−0.625(2)[012]
108	0	2194.0(22)[046]	−588.2(13)[23]	−0.510(1)[009]
109	5/2	1958.3(22)[038]	−515.3(06)[21]	−0.445(1)[009]
110	0	1432.2(23)[030]	−382.4(05)[15]	−0.334(1)[006]
111	1/2	1314.3(22)[023]	−334.4(13)[10]	−0.288(1)[012]
112	0	674.6(22)[015]	−182.8(04)[07]	−0.159(1)[004]
113	1/2	555.2(23)[008]	−134.3(08)[09]	−0.114(1)[010]
114	0	0.0(0)[000]	0.0(00)[00]	0.000(0)[000]
115	1/2	−110.4(29)[007]	47.3(11)[06]	0.043(1)[012]
116	0	−526.5(22)[015]	151.5(07)[07]	0.134(1)[008]
117	1/2		192.9(11)[21]	0.171(2)[020]
118	0		275.5(20)[14]	0.243(3)[022]
119	1/2		319.0(10)[32]	0.283(3)[033]
120	0		386.5(10)[21]	0.342(3)[037]
121	3/2	−1309.3(40)[050]	420.9(09)[31]	0.375(4)[049]
122	0		484.9(11)[27]	0.431(5)[054]
123	3/2	−1551.5(37)[065]	514.0(17)[39]	0.457(6)[067]
124	0	−1748.2(22)[072]	574.9(33)[34]	0.510(6)[072]
125	3/2	−1757.3(35)[079]		0.533(7)[086]
126	0	−1957.6(22)[086]	657.0(38)[40]	0.585(8)[090]
127	3/2	−1912.3(30)[094]		0.599(9)[106]
128	0	−2171.6(23)[100]		0.660(9)[107]
129	3/2	−1911.1(55)[108]		0.638(12)[133]
130	0	−2208.1(33)[115]		0.705(11)[132]

charge radii and higher moments $\delta\langle r^n\rangle^{A,A'}$ are derived from Barrett equivalent radii $R_{\text{K}\alpha}^\mu$ using $\langle r^n\rangle = (R_{\text{k}\alpha}^\mu/V_n)^n$, $n = 2$, 4, 6 with V_n values obtained from elastic electron scattering and listed in [5] for all stable Cd isotopes. For Cd, $\lambda^{114,A}$ deviates by about –2.7% from the respective $\delta\langle r^2\rangle$.

Figure 1 shows the modified isotope shift as a function of the modified size parameter for the stable isotopes. We perform a linear regression to obtain the slope and the intercept, representing the field-shift and the mass-shift constants, respectively, which are required to extract the charge radii of the radioactive isotopes. We have used the procedure described in [38], which provides unified standard error estimates when taking into account uncertainties in both directions. The uncertainty of the mass-shift
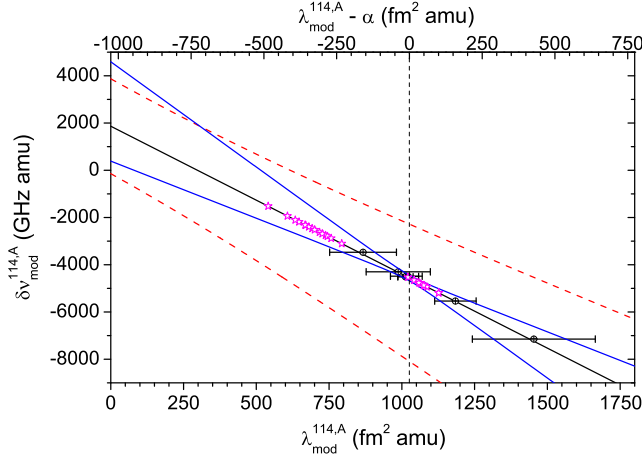
FIG. 1. King plot of the Cd II data showing the results for the stable isotopes with uncertainties based on the charge radii from muonic atoms, the regression line, and the confidence intervals based on the (standard) regression (dashed, red) and the one that removes the correlation between the intercept and the slope by shifting the x axis by 1026 fm^2 amu (solid, blue). Stars (magenta) indicate the positions of the unstable isotopes in the King plot ($A > 114$ with $\lambda_{\mathrm{mod}} < 800$ fm^2 amu, $A < 114$ with $\lambda_{\mathrm{mod}} > 1000$ fm^2 amu).

FIG. 2. Experimental nuclear charge radii along the Cd isotopic chain compared with theoretical predictions from different nuclear DFT models: SV-min from the Skyrme functionals [40], Fy(Δr) from the Fayans functionals [25], and the relativistic functional FSU-Garnet that was optimized on a global set of rms charge radii data taken from [42] (including Cd) employing a Bayesian neural network (BNN) approach [27]. The gray band represents the systematic uncertainty of the experimental results due to the uncertainty of the field-shift constant F. The inset shows the corresponding one-neutron separation energies from experiment [36] and nonrelativistic DFT.

constant $K_{\mathrm{ion}} = 1860(1920)$ GHz amu is large and is strongly correlated with the slope of the line, for which $F_{\mathrm{ion}} = -6260(1860)$ MHz/fm^2 is obtained in excellent agreement with the result of a semiempirical approach of $F_{\mathrm{se,ion}} = -6124(772)$ MHz/fm^2 presented in [39]. Simple Gaussian error propagation leads to the confidence band shown as a dashed red curve, producing large uncertainties for the extracted size parameters. However, the modified isotope shifts of the unstable isotopes cluster around those of the stable isotopes, where the line is much better determined than represented by the uncertainty interval. This is particularly true for the neutron deficient ones as indicated in the figure. One option to improve the procedure is to propagate the errors including the full covariance matrix. Alternatively, the simple linear transformation $x \to (x - \alpha)$ shifts the y axis into the center of the distribution and therefore reduces the correlation between the two degrees of freedom to almost zero for $\alpha = 1026$ fm^2 amu. This leads to a modified y-axis intercept of $K_{1026} = -4561(115)$ GHz amu and the $1 - \sigma$ confidence band shown in blue in Fig. 1.

By transforming Eq. (1) accordingly, solving for λ and applying K_{1026} and F, we obtain the nuclear size parameter for all isotopes according to

$$\lambda^{A,A'} = (\delta\nu^{A,A'} - K_\alpha\mu)/F + \alpha/\mu. \qquad (3)$$

The isotope shift determined in the Cd I transition is projected onto the Cd II transition by performing a King plot between the isotope shifts of both transitions. The projected isotope shift is then used to calculate λ of those isotopes for which Cd II data are unavailable. The excellent agreement between the results from both transitions for all other isotopes confirms the compatibility of the data. Combined results are listed in Table I, where the systematic uncertainty of the rms charge radii is based on the uncertainty of F. A -2.7% contribution of the higher moments to λ was adopted for all isotopes.

Charge radii were calculated from $\lambda^{114,A}$ based on the reference radius of $R(^{114}\mathrm{Cd}) = 4.612(1)$ fm [5] and are compared with predictions from nuclear DFT in Fig. 2. From the nonrelativistic models, we consider the Skyrme functional SV-min [40] and the Fayans functional Fy(Δr) [25]. The latter is in most respects very similar to Skyrme but has two crucial extensions: a gradient term within the surface term and a gradient term in the pairing functional. Besides the Skyrme functional, we have also checked two parametrizations with other functional forms, the Fayans functional Fy(std) [25] and a density-dependent relativistic model RMF-DD [41], both fitted to the same set of data as SV-min. Both yield practically the same result as SV-min and are thus not shown explicitly in Fig. 2. Additionally, we consider one example for a relativistic mean-field model (RMF, FSU-Garnet) and take here the most recent BNN fit to charge radii residuals which took care to achieve a good global fit of nuclear radii [27]. All DFT models, except Fy(Δr), fail to reproduce the isotopic trend as a whole and the odd-even staggering in detail. The reason is that neither the standard Skyrme model nor the RMF has a sufficiently

flexible pairing functional to cope with the given trends. The two new gradient terms in the Fayans functional make the difference. But that is not the whole story. The Fayans parametrization Fy(std) [25] that employed the same large standard set of data for the calibration of the model as SV-min [40] fails similarly to SV-min. While this data set does not contain constrains on differential radii, the set for Fy(Δr) had been extended by particular information on differential radii in the Ca chain. This activates the gradient terms, which are crucial to adapt the trends. The gratifying surprise is that this parametrization, tuned to the Ca chain, performs very well also for the Cd chain. This confirms nicely that isotopic trends of charge radii share common features that require more elaborate pairing functionals. In turn, systematics of precision data on rms charge radii will become extremely useful for the further development of pairing within nuclear DFT, an aspect which is presently not fully under control. It should also be noted that the odd-even staggering in the radii as well as in the one-neutron binding energies S_{1n} (inset in Fig. 2) is slightly exaggerated, as is also the case in the calcium chain. Moreover, the Fy(Δr) functional predicts a more pronounced kink at $N = 82$, followed by a steep increase in charge radii, than the other functionals. This calls for an experimental investigation of nuclear charge radii beyond ^{130}Cd.

In summary, isotope shifts of Cd isotopes were measured along almost the complete $sdgh$ shell and differences in mean-square nuclear charge radii have been extracted and compared to density functional theory predictions. A surprising consistency with the prediction of a newly proposed Fayans parametrization Fy(Δr) functional that was developed to explain the trends of charge radii in the Ca chain was found, while other functionals largely fail to reproduce the data.

[*]wnoertershaeuser@ikp.tu-darmstadt.de

[†]Present address: Extreme Light Infrastructure Nuclear Physics, Horia Hulubei National Institute for R&D in Physics and Nuclear Engineering, Bucharest-Magurele 077125, Romania.

[‡]Present address: Department of Physics, Tennessee Technological University, Cookeville TN, 38505, USA.

[1] G. Gamow, Proc. R. Soc. A **126**, 632 (1930).
[2] C. F. v. Weizsäcker, Z. Phys. **96**, 431 (1935).
[3] J. L. Friar and J. W. Negele, *Theoretical and Experimental Determination of Nuclear Charge Distributions*, edited by M. Baranger and E. Vogt, Advances in Nuclear Physics Vol. 8 (Springer, Boston, MA 1975), p. 219.
[4] J. Friedrich and N. Voegler, Nucl. Phys. **A373**, 192 (1982).
[5] G. Fricke and K. Heilig, *Nuclear Charge Radii* (Landolt-Börnstein/Springer, Berlin, 2004).
[6] I. Angeli and K. P. Marinova, At. Data Nucl. Data Tables **99**, 69 (2013).
[7] R. Neugart, Hyperfine Interact. **24**, 159 (1985).
[8] E. W. Otten, *Nuclear Radii and Moments of Unstable Isotopes*, edited by D. A. Bromley, Treatise on Heavy Ion Science Vol. 8 (Springer, Boston, MA, 1989) p. 517.
[9] K. J. Pototzky, J. Erler, P.-G. Reinhard, and V. O. Nesterenko, Eur. Phys. J. A **46**, 299 (2010).
[10] N. Schunck, J. Dobaczewski, J. McDonnell, J. Moré, W. Nazarewicz, J. Sarich, and M. V. Stoitsov, Phys. Rev. C **81**, 024316 (2010).
[11] B. Bally, B. Avez, M. Bender, and P.-H. Heenen, Phys. Rev. Lett. **113**, 162501 (2014).
[12] R. J. Furnstahl, Nucl. Phys. **A706**, 85 (2002).
[13] P.-G. Reinhard and W. Nazarewicz, Phys. Rev. C **81**, 051303(R) (2010).
[14] J. Piekarewicz, B. K. Agrawal, G. Colò, W. Nazarewicz, N. Paar, P.-G. Reinhard, X. Roca-Maza, and D. Vretenar, Phys. Rev. C **85**, 041302(R) (2012).
[15] P.-G. Reinhard and W. Nazarewicz, Phys. Rev. C **93**, 051303(R) (2016).
[16] T. Hashimoto *et al.*, Phys. Rev. C **92**, 031305(R) (2015).
[17] W. von Oertzen, M. Freer, and Y. Kanada En'yo, Phys. Rep. **432**, 43 (2006).
[18] J. S. Al-Khalili, J. A. Tostevin, and I. J. Thompson, Phys. Rev. C **54**, 1843 (1996).
[19] G. Hagen, A. Ekström, C. Forssén, G. R. Jansen, W. Nazarewicz, T. Papenbrock, K. A. Wendt, S. Bacca, N. Barnea, B. Carlsson, C. Drischler, K. Hebeler, M. Hjorth-Jensen, M. Miorelli, G. Orlandini, A. Schwenk, and J. Simonis, Nat. Phys. **12**, 186 (2016).
[20] A. Ekström, G. R. Jansen, K. A. Wendt, G. Hagen, T. Papenbrock, B. D. Carlsson, C. Forssén, M. Hjorth-Jensen, P. Navrátil, and W. Nazarewicz, Phys. Rev. C **91**, 051301(R) (2015).
[21] M. Bender, P.-H. Heenen, and P.-G. Reinhard, Rev. Mod. Phys. **75**, 121 (2003).
[22] F. R. Garcia Ruiz *et al.*, Nat. Phys. **12**, 594 (2016).
[23] S. A. Fayans, JETP Lett. **68**, 169 (1998).
[24] S. Fayans, S. Tolokonnikov, E. Trykov, and D. Zawischa, Nucl. Phys. **A676**, 49 (2000).
[25] P.-G. Reinhard and W. Nazarewicz, Phys. Rev. C **95**, 064328 (2017).
[26] K. Minamisono, D. M. Rossi, R. Beerwerth, S. Fritzsche, D. Garand, A. Klose, Y. Liu, B. Maaß, P. F. Mantica, A. J. Miller, P. Müller, W. Nazarewicz, W. Nörtershäuser, E. Olsen, M. R. Pearson, P.-G. Reinhard, E. E. Saperstein, C. Sumithrarachchi, and S. V. Tolokonnikov, Phys. Rev. Lett. **117**, 252501 (2016).
[27] R. Utama, W.-C. Chen, and J. Piekarewicz, J. Phys. G **43**, 114002 (2016).

[28] M. J. G. Borge and B. Jonson, J. Phys. G **44**, 044011 (2017).

[29] U. Köster, O. Arndt, E. Bouquerel, V. N. Fedoseyev, H. Frånberg, A. Joinet, C. Jost, I. S. K. Kerkines, and R. Kirchner (The TARGISOL Collaboration), Nucl. Instrum. Methods Phys. Res., Sect. B **266**, 4229 (2008).

[30] R. Neugart, J. Billowes, M. L. Bissell, K. Blaum, B. Cheal, K. T. Flanagan, G. Neyens, W. Nörtershäuser, and D. T. Yordanov, J. Phys. G **44**, 064002 (2017).

[31] K. Kreim, M. L. Bissell, J. Papuga, K. Blaum, M. De Rydt, F. R. Garcia Ruiz, S. Goriely, H. Heylen, M. Kowalska, R. Neugart, G. Neyens, W. Nörtershäuser, M. M. Rajabali, R. Sánchez Alarcón, H. H. Stroke, and D. T. Yordanov, Phys. Lett. B **731**, 97 (2014).

[32] H. Frånberg, P. Delahaye, J. Billowes, K. Blaum, R. Catherall, F. Duval, O. Gianfrancesco, T. Giles, A. Jokinen, M. Lindroos, D. Lunney, E. Mane, and I. Podadera, Nucl. Instrum. Methods Phys. Res., Sect. B **266**, 4502 (2008).

[33] N. Frömmgen, D. L. Balabanski, M. L. Bissell, J. Bieroń, K. Blaum, B. Cheal, K. Flanagan, S. Fritzsche, C. Geppert, M. Hammen, M. Kowalska, K. Kreim, A. Krieger, R. Neugart, G. Neyens, M. M. Rajabali, W. Nörtershäuser, J. Papuga, and D. T. Yordanov, Eur. Phys. J. D **69**, 164 (2015).

[34] D. T. Yordanov, D. L. Balabanski, J. Bieroń, M. L. Bissell, K. Blaum, I. Budinčević, S. Fritzsche, N. Frömmgen, G. Georgiev, C. Geppert, M. Hammen, M. Kowalska, K. Kreim, A. Krieger, R. Neugart, W. Nörtershäuser, J. Papuga, and S. Schmidt, Phys. Rev. Lett. **110**, 192501 (2013).

[35] D. T. Yordanov et al., Phys. Rev. Lett. **116**, 032501 (2016).

[36] M. Wang, G. Audi, F. Kondev, W. Huang, S. Naimi, and X. Xu, Chin. Phys. C **41**, 030003 (2017).

[37] G. Fricke, C. Bernhardt, K. Heilig, L. Schaller, L. Schellenberg, E. Shera, and C. de Jager, At. Data Nucl. Data Tables **60**, 177 (1995).

[38] D. York, N. M. Evensen, M. L. Martnez, and J. D. B. Delgado, Am. J. Phys. **72**, 367 (2004).

[39] J. Bauche, H. Hühnermann, D. N. Stacey, V. Stacey, and M. Wilson, Z. Phys. A **320**, 157 (1985).

[40] P. Klüpfel, P.-G. Reinhard, T. J. Bürvenich, and J. A. Maruhn, Phys. Rev. C **79**, 034310 (2009).

[41] W. Nazarewicz, P.-G. Reinhard, W. Satuła, and D. Vretenar, Eur. Phys. J. A **50**, 20 (2014).

[42] I. Angeli, At. Data Nucl. Data Tables **87**, 185 (2004).